Scripta Materialia 136 (2017) 46–49

Contents lists available at ScienceDirect

Scripta Materialia

journal homepage: www.elsevier.com/locate/scriptamat

Transformations of α' martensite in Ti–Fe alloys under high pressure torsion

A. Kilmametov [a], Yu Ivanisenko [a], B. Straumal [a,b,c,*], A.A. Mazilkin [a,b], A.S. Gornakova [b], M.J. Kriegel [d], O.B. Fabrichnaya [d], D. Rafaja [d], H. Hahn [a]

[a] Karlsruhe Institute of Technology (KIT), Institute of Nanotechnology, Hermann-von-Helmholtz-Platz 1, 76344 Eggenstein-Leopoldshafen, Germany
[b] Institute of Solid State Physics, Russian Academy of Sciences, Ac. Ossipyan str. 2, 142432 Chernogolovka, Russia
[c] Laboratory of Hybrid Nanomaterials, National University of Science and Technology «MISIS», Leninskii prosp. 4, 119049 Moscow, Russia
[d] TU Bergakademie Freiberg, Institute of Materials Science, Gustav-Zeuner-Straße 5, 09599 Freiberg, Germany

ARTICLE INFO

Article history:
Received 28 December 2016
Received in revised form 5 April 2017
Accepted 7 April 2017
Available online xxxx

Keywords:
Nano-crystalline metals
Microstructure
Thermodynamics and kinetics
Ti–Fe alloy
High-pressure torsion

ABSTRACT

Phase transitions in α'-Ti martensite driven by high pressure torsion (HPT) as well as α' → ω transformations in Ti–Fe alloys were observed for the first time. The as cast alloys transformed into α'-Ti martensite after annealing in the β-(Ti,Fe) solid solution region and subsequent quenching. Lattice parameters of α'-Ti martensite decreased with increasing iron content, similar to the lattice parameter of β-Ti. During HPT, α'-Ti martensite transformed partly into ω-Ti. At the same time, the lattice parameters of remaining α'-Ti phase increased towards those for iron-free α-Ti. These processes included an increased mass transfer of iron atoms out of α'-Ti.

1. Introduction

Titanium and titanium alloys are attractive materials for various applications due to their high strength-to-density ratio, excellent corrosion resistance, and good biocompatibility [1]. Nevertheless, further improvement of the Ti alloys is very important. Severe plastic deformation (SPD) revealed to be a principally new instrument for improvement of their capability. SPD results in substantial grain refinement [2] as well as initiates various phase transformations, such as formation or decomposition of a supersaturated solid solutions, dissolution of phases, amorphization of crystalline phases or formation of nanocrystals during decomposition of amorphous phase [3,4]. Particularly, the SPD-induced peculiarities of microstructure provide unique mechanical properties of Ti and Ti-based alloys [5–7]. In such a way, SPD acts in an advanced capacity that allows the structure and properties of Ti alloys to be tailored.

As well known, high pressure torsion (HPT) is a technique of SPD that give rise to appearance of high-pressure ω-phase in Ti, Zr and a number of their alloys [5–7]. However, not only α, β and ω phases are involved in these transformations [8]. At low concentrations of β-stabilizing elements in titanium alloys, the hexagonal closely packed (hcp) α' martensite (space group $P6_3/mmc$) or the orthorhombic α'' martensite (space group Cmcm) [9] can be created from the body centred cubic (bcc) β-phase at high cooling rate [10–16]. Usually, the α'' martensite appears at higher concentrations of alloying elements [17,18]. Several authors reported that the presence of α' and α'' martensites in the microstructure of the Ti-based alloys strongly influences their properties [10–16]. However, still there is a lack of knowledge regarding the influence of SPD on α'-Ti or α''-Ti martensites. Therefore, the goal of this work is to study the effect of HPT on the transformations of α' martensite in Ti–Fe alloys with low iron content.

2. Experimental

Pure titanium and four Ti–Fe alloys with 0.5, 1, 2.2 and 4 wt% Fe were investigated. The alloys were inductively melted in vacuum starting from high purity components (99.9% Ti and 99.97% Fe). The samples were sealed into evacuated silica ampoules with a residual pressure of approximately 4×10^{-4} Pa. Samples were annealed at 950 °C for 104 h and then quenched into the ice-water. Then they were deformed by HPT in a Bridgman anvil type unit (295 K, 7 GPa,) using a custom built device (W. Klement GmbH, Lang, Austria). The disks of 10 mm in diameter and approximately 0.35 mm in thickness were prepared. After HPT, the central (about ø3 mm) part of each ø10 mm disk was excluded from further investigations.

Torsion straining of a disc sample of diameter *2R* and thickness *t* produces a shear strain γ

* Corresponding author at: Institute of Solid State Physics, Russian Academy of Sciences, Chernogolovka, Moscow District 142432, Russia.
E-mail address: straumal@issp.ac.ru (B. Straumal).

http://dx.doi.org/10.1016/j.scriptamat.2017.04.010
1359-6462/

$$\gamma = 2\pi n\, r/t \quad (1)$$

n being the number of rotations of the mobile anvil, r being the distance from the sample centre. γ varies from zero on the sample axis to a maximum value γ_{max} on the lateral surface (situated at a distance $r = R$ from the axis). For comparison of shear deformation with tensile strain, the equivalent strain value e_{eq} can be used [19,20]:

$$e_{eq} = \gamma/\sqrt{3} = 2\pi nr/t\sqrt{3} \quad (2)$$

All samples for the investigations were cut from the deformed disks at a distance of $r = 3$ mm from the sample centre. For this distance and 0.1 anvil rotations the shear strain $\gamma = 5.4$ and the equivalent strain value $e_{eq} = 3.1$. For 5 anvil rotations $\gamma = 270$ and $e_{eq} = 156$, respectively. This strain value has been typically used for the production of nanograined materials in earlier studies [19–21].

Scanning electron microscopy (SEM) investigations have been carried out in a Tescan Vega TS5130 MM microscope equipped with the LINK energy-dispersive spectrometer produced by Oxford Instruments. Transmission electron microscopy (TEM) observations have been made by using an aberration corrected TITAN 80-300 microscope. The specimens were cut at half of radius of the HPT disk and further thinned in a FEI Strata 400S dual beam facility. X-ray diffraction (XRD) patterns have been obtained in the symmetrical Bragg–Brentano geometry using Philips X'Pert powder diffractometer with the Cu-K_α anode. The XRD peak profiles were fitted by Pseudo-Voigt function. Lattice parameter evaluation was performed by the Fityk software [22] using a Rietveld-like whole profile refinement.

3. Results and discussion

The solubility of Fe in α-Ti at room temperature is about 0.03–0.05 wt% [23–26]. By quenching a β-(Ti-Fe) solid solution with the Fe content below 4 wt%, the hexagonal α' martensite with space group $P6_3/mmc$ forms [27–35]. According to Dobromyslov et al. [17,18], the orthorhombic α'' (space group Cmcm) does not appear in Ti–Fe alloys. At higher Fe contents (>4 wt% Fe), the metastable bcc β-Ti phase can be retained after quenching [27–35]. Fig. 1a shows the Ti-rich part of the Ti–Fe phase diagram with the dotted line of β → α' martensitic transformation and a schematic diagram showing the Pitsch-Schrader (PS) orientation relationship between β-(Ti-Fe) austenite and α' martensite [27–35]. Large open squares in Fig. 1a show the annealing temperature and compositions of the studied alloys.

In Fig. 1b, a SEM micrograph of Ti–1 wt% Fe alloy after annealing at 950 °C and subsequent quenching is shown. Decomposition of the high temperature bcc β-phase upon cooling may proceed via diffusional, shear or mixed diffusional and shear modes [36]. Typical acicular martensite plates (Fig. 1b) clearly indicate the diffusionless shear mode of transformation. The growth of primary α' martensitic plates was restricted by the boundaries of β-grains. The length of the longest martensitic plates was about 200 μm. Only primary and secondary martensite plates are visible in Fig. 1b, similar to the quenched Ti–Mo alloys [37]. The primary and secondary martensite plates are marked in the left upper corner of the micrograph in Fig. 1b by white lines and digits 1 and 2, respectively. Tertiary and quaternary α' martensite plates are not visible in our case. A small amount of retained β-phase is located between α' martensite plates. According to the TEM micrograph of the Ti–1 wt% Fe alloy after HPT (Fig. 1c,d), the initial grain structure was completely transformed. It consisted now of a mixture of very fine (~100–200 nm) equiaxial grains of α'-Ti and ω-Ti phases.

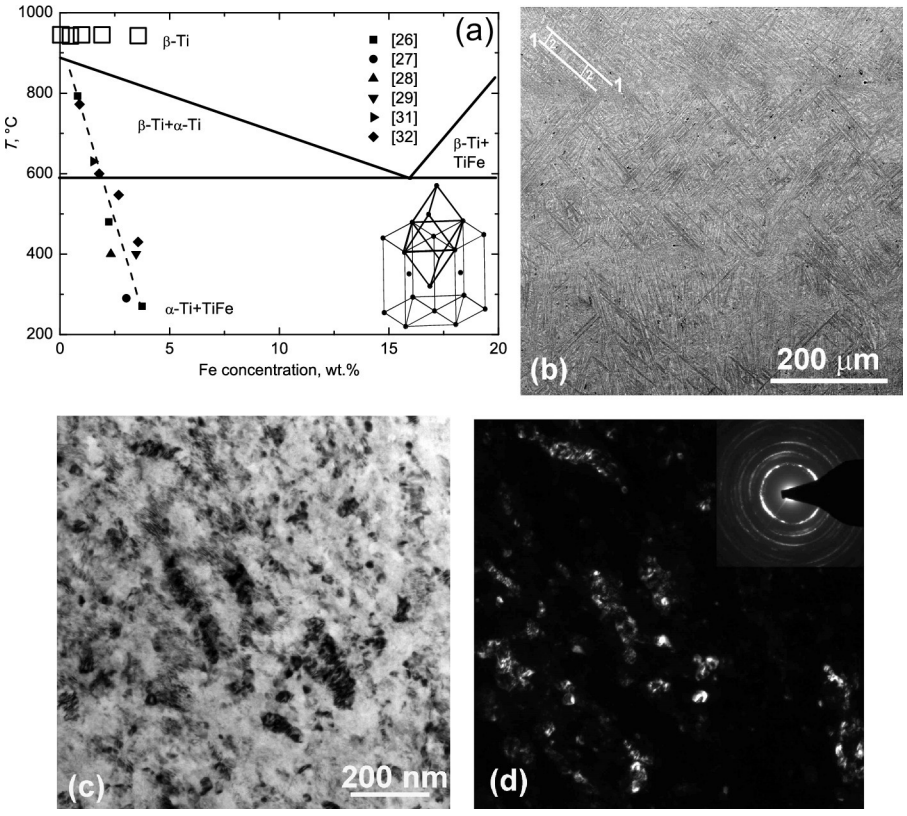

Fig. 1. (a) Ti-rich part of the Ti–Fe phase diagram with the dotted line of β-α' martensitic transformation [32]. Large open squares show the annealing temperature and compositions of studied alloys. Inset shows the orientation relationship between β and α phases [32]. (b) SEM micrograph of Ti–1 wt% Fe alloy after annealing at 950 °C and quenching. The primary and secondary martemsite plates are marked in the left upper corner by white lines and digits 1 and 2, respectively. (c) bright field and (d) dark field TEM micrographs of Ti–1 wt% Fe alloy after annealing at 950 °C, quenching and HPT.

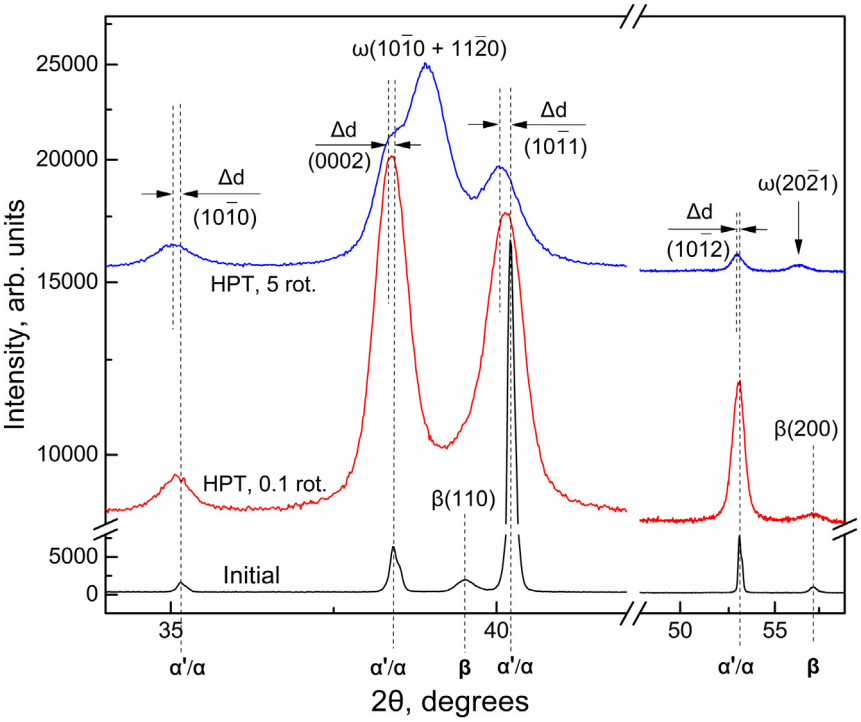

Fig. 2. X-ray diffraction patterns of Ti–1 wt% Fe alloy after annealing at 950 °C and quenching (bottom curve), after HPT for 0.1 rotation (middle curve) and after HPT for 5 rotations (top curve). The patterns are vertically shifted for better comparison.

The lower curve in Fig. 2 shows the XRD patterns of the as-quenched coarse-grained Ti–1 wt% Fe alloy. The set of narrow peaks indicates mainly α-Ti and/or α' martensite with hcp lattice and a small amount of bcc β-Ti. In general, XRD patterns of α-Ti and α'-Ti martensite are very similar, because these phases belong to the same space group. However, they can be distinguished by the measurements of lattice parameters [38]. XRD peak profiles of the HPT-processed Ti–1 wt% Fe alloy are substantially broadened due to strong refinement of the microstructure and a high density of lattice defects.

After HPT at 7 GPa and 0.1 rotation (middle curve in Fig. 2) the redistribution of the XRD peaks integral intensities took place. It happened due to development of shear deformation texture. Such shear-driven texture has been reported earlier for HPT-processed commercially pure Ti [6]. The $(0002)_\alpha$ peak had the strongest intensity under shear stress conditions (Fig. 2). This fact implies preferable atomic shuffling along $(0001)_\alpha$ planes. In turn, this shuffling facilitated α to ω transformation according to orientation relationships between these two phases: $(0001)_\alpha \parallel (0\bar{1}11)_\omega$ or $(0001)_\alpha \parallel (11\bar{2}0)_\omega$ [39–41].

Applying HPT for 5 rotations (upper curve in Fig. 2) resulted in the massive formation of the ω-phase and simultaneous disappearance of the β-phase. The α' peaks shifted during HPT to lower diffraction angles. Thus, Fig. 2 shows clearly pronounced changes in the interplanar spacings Δd for the hcp lattice. These changes corresponded to the increase of lattice parameters and to the decrease of the Fe content in α' phase. After HPT for 5 rotations, the majority of α-Ti transformed into ω-Ti (space group P6/mmm) in all the studied alloys. Only minor amount of α-Ti remained, whereas β-Ti completely disappeared. One can assume that the remained α phase did not form in the studied alloys after quenching but appeared after the HPT treatment. As a result of shear deformation under imposed high pressure, phase transformations took place, at which the $(\alpha' + \beta)$ phase mixture rearranged to $(\alpha + \omega)$ one. From the integral intensities of XRD peaks, the amount of α'/α- and ω-phases in Ti–1 wt% Fe alloy can be roughly estimated to be 35–40% and 60–65%, respectively. Taking into account that only 10–15% of the β-phase was present in the initial state, it is reasonable to consider that α' or α mainly transformed to the ω phase. Fig. 2 illustrates the results of HPT induced transformations in Ti–Fe alloys, indicating noticeable increases of hcp lattice parameters without any ω-phase creation after 0.1 rotation (Fig. 2, middle curve). Therefore, our results point towards the following sequence of phase transformations: α' → α and α → ω in Ti—Fe alloys at HPT.

The solubility of Fe in β-Ti is high, but in α-Ti it does not exceed 0.05 wt%. The addition of Fe decreases the lattice parameter of β-Ti [42–45]. The lattice parameters *a* and *c* of the α' martensite in as-quenched Ti–0.5 to 4 wt% Fe alloys also decreased (Fig. 3a, b). We have to underline here that the conditions of HPT processing used for the different measurements of lattice parameters for all studied alloys in Fig. 3 did not change. The lattice parameters *a* and *c* exhibited their minimal values in the range of 0.5–1 wt% Fe thus indicating maximal contribution of the α' martensite to the lattice contraction observed. During HPT, α'-Ti martensite transformed into the mixture of ω- and α-phases (Fig. 2). For minor Fe contents, parameters *a* (Fig. 3a) and *c* (Fig. 3b) of the hcp lattice increased up to the level of pure α-Ti subjected to HPT. For 2 and 4 wt% Fe in Ti, HPT caused mainly a decrease of the lattice parameters with increasing of Fe content (Fig. 3a, b). As compared to a pure Ti or minor percentage of Fe, this indicates slightly enhanced solubility in α phase induced by HPT. Thus, HPT decreases the iron content in the α'-Ti martensite, "purifies" it and drives the α' → α transformation. Therefore, HPT of α'-Ti martensite included the accelerated mass-transfer similar to that observed under HPT of Al- and Cu-based alloys [46–49]. The reason of accelerated diffusion during HPT is not only the shear-driven atom movement but also the extremely high concentration of non-equilibrium vacancies [50–52].

The precise XRD measurements shown that SPD produces vacancies and/or vacancy-like defects in very high densities which are typically close to those of vacancies in thermal equilibrium at the melting point [53,54]. The main influence of increased vacancy content reflected itself in the background intensity of X-ray diffraction patterns [53,54]. Nevertheless, one can expect that the high concentrations of defects may also influence the positions of X-ray peaks, i.e. the lattice parameters measured. The important indication for such possible influence are the observed differences in *a* and *c* parameters before and after HPT for pure

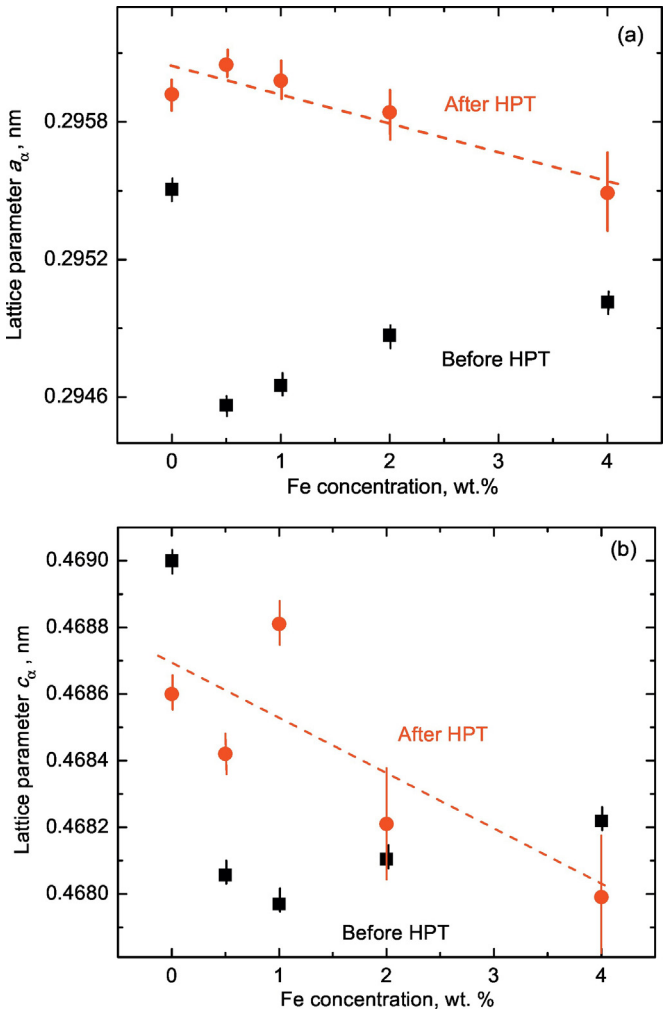

Fig. 3. Dependencies of the lattice parameters (a) *a* and (b) *c* in the α/α'-phase before (squares) and after (circles) HPT (7 GPa, 5 rot.) on the iron concentration on studied Ti–Fe alloys. Lines are the guide for the eye.

titanium, i.e. even without iron (see Fig. 3). It is known also that (with the same deformation parameters chosen) the density of deformation induced defects increases with increasing alloy content [55]. This effect can also slightly influence the observed phenomena.

Taking into account low solubility of Fe in α phase, it is reasonable to propose that Fe atoms are mostly dissolved in ω phase. Thus, the evaluation of the lattice parameters for ω phase enables to estimate the input of Fe content to the changes of the atomic volume per unit cell of this phase. For Ti-4 wt% Fe alloy, both lattice parameters of ω phase were reduced ($a = 0.4610$ nm, $c = 0.2825$ nm) in comparison with the ω phase in commercially pure HPT Ti ($a = 0.4627$ nm, $c = 0.2830$ nm). Corresponding reduction of the atomic volume achieves 0.9%, that is comparable, for example, with the difference between α and β phase atomic volumes. Decrease of the unit cell parameters correlates well with the effect of Fe on the β phase lattice parameter and can be used as a measure for the solubility of Fe in ω phase.

4. Conclusions

In this work we observed for the first time the phase transitions in α'-Ti martensite as well as α'Ti → ωTi transformations driven by the HPT in Ti–Fe alloys. After annealing in the β-(Ti,Fe) solid solution region and subsequent quenching, the as-cast Ti–Fe alloys with 0.5, 1, 2.2 and 4 wt% Fe transformed into the hexagonal α'-Ti martensite. The lattice parameters of α'-Ti martensite in as-quenched Ti-Fe alloys decreased with increasing Fe content in an alloy. After HPT, the lattice parameters of α'-Ti increased towards those for pure α-Ti, and the majority of α'-Ti transformed into ω-Ti. This process includes an accelerated mass transfer of iron atoms out of α'-Ti.

Acknowledgements

This work was partially supported by the Ministry of Education and Science of the Russian Federation in the framework of the Program to Increase the Competitiveness of NUST "MISiS" (К2-2014-013 and K2-2015-073), by the Deutsche Forschungsgemeinschaft, by the Russian Foundation for Basic Research (grants 16-53-12007 and 16-03-00285) as well as by the Karlsruhe Nano Micro Facility (KNMF, www.knmf.kit.edu).

References

[1] M.J. Donachie Jr., Titanium: A Technical Guide, second ed. ASM International, Materials Park, OH, USA, 2000.
[2] R.Z. Valiev, R.K. Islamgaliev, I. Alexandrov, Prog. Mater. Sci. 45 (2000) 103.
[3] X. Sauvage, A. Chbihi, X. Quelennec, J. Phys. 240 (2010) 012003.
[4] B. Straumal, A. Korneva, P. Zięba, Arch. Civ. Mech. Eng. 14 (2014) 242.
[5] B.B. Straumal, A.R. Kilmametov, Yu. Ivanisenko, et al., Adv. Eng. Mater. 17 (2015) 1835.
[6] Y. Ivanisenko, A. Kilmametov, H. Roesner, et al., Int. J. Mater. Res. 99 (2008) 36.
[7] B.B. Straumal, A.S. Gornakova, A.A. Mazilkin, et al., Mater. Lett. 81 (2012) 225.
[8] A. Panigrahi, M. Bönisch, T. Waitz, et al., J. Alloys Compd. 628 (2015) 434.
[9] N. Dai, L.-C. Zhang, J. Zhang, et al., Corros. Sci. 111 (2016) 703.
[10] J.L. Murray, Phase Diagrams of Binary Titanium Alloys, second ed. ASM International, Metals Park, Ohio, USA, 1987.
[11] J. Xu, W. Zeng, Y. Zhao, et al., J. Alloys Compd. 688 (2016) 301.
[12] K.-M. Hong, Y.C. Shin, J. Mater. Process. Technol. 237 (2016) 420.
[13] J. Yang, H. Yu, J. Yin, et al., Mater. Des. 108 (2016) 308.
[14] P. Zhao, L. Fu, H. Chen, J. Alloys Compd. 675 (2016) 248.
[15] Q. Zhang, J. Chen, H. Tan, et al., Trans. Nonferrous Metals Soc. China 26 (2016) 2058.
[16] M.M. Stupel, M. Ron, B.Z. Weiss, J. Appl. Phys. 47 (1976) 6.
[17] A.V. Dobromyslov, V.A. Elkin, Scr. Mater. 44 (2001) 905.
[18] A.V. Dobromyslov, V.A. Elkin, Mater. Sci. Eng. A 438 (2006) 324.
[19] R.Z. Valiev, Yu.V. Ivanisenko, E.F. Rauch, B. Baudelet, Acta Metall. 44 (1996) 4705.
[20] A.V. Korznikov, G. Tram, O. Dimitrov, G.F. Korznikova, S.R. Idrisova, Z. Pakiela, Acta Mater. 49 (2001) 663.
[21] B.B. Straumal, B. Baretzky, A.A. Mazilkin, F. Phillipp, O.A. Kogtenkova, M.N. Volkov, R.Z. Valiev, Acta Mater. 52 (2004) 4469.
[22] M. Wojdyr, J. Appl. Crystallogr. 43 (2010) 1126.
[23] N.G. Boriskina, K.P. Myasnikova, Dokl. Akad. Nauk SSSR 7 (1962) 61.
[24] E. Raub, C.J. Raub, E. Roeschel, J. Less-Common Met. 12 (1967) 36.
[25] A. Blaesius, U. Gonser, J. Phys. Colloq. 37 (1976) C6–397.
[26] J. Matyka, F. Faudot, J. Bigot, Scr. Metall. 13 (1979) 645.
[27] W. Pitsch, A. Schrader, Arch. Eisenhüttenwes. 29 (1958) 715.
[28] U. Dahmen, Acta Metall. Mater. 30 (1982) 63.
[29] H. Kaneko, Y.C. Huang, J. Jpn. Inst. Metals 27 (1963) 1393.
[30] V.N. Moiseev, Met. Sci. Heat Treat. 5 (1969) 335.
[31] T. Sato, S. Hukai, Y.C. Huang, J. Austral. Inst. Met. 5 (1960) 149.
[32] P. Duwez, Trans. Am. Soc. Met. 45 (1953) 934.
[33] D.H. Polonis, J.G. Parr, Trans. Am. Inst. Min. Met. Eng. 200 (1954) 1148.
[34] Y.N. Gridnev, Yu.N. Petrov, V.A. Rafalovskiy, et al., Vopr. Fiz. Met. Metalloved. AN UkrSSR Sb. Nauchn. Rabot. 11 (1960) 82 (In Russian).
[35] J.L. Murray, Bull. Alloy Phase Diagr. 2 (1981) 320.
[36] R. Davis, H.M. Flower, D.R.F. West, J. Mater. Sci. 14 (1979) 712.
[37] Z. Tarzimoghadam, S. Sandlöbes, K.G. Pradeep, et al., Acta Mater. 97 (2015) 291.
[38] F.F. Cardoso, A. Cremasco, R.J. Contieri, et al., Mater. Des. 32 (2011) 4608.
[39] J.M. Silcock, Acta Metall. 6 (1958) 481.
[40] M.P. Usikov, V.A. Zilbershtein, Phys. Status Solidi A 19 (1973) 53.
[41] D.R. Trinkle, R.G. Hennig, S.G. Srinivasan, et al., Phys. Rev. Lett. 91 (2003) 025701.
[42] R. Ray, B.C. Giessen, N.J. Grant, Metall. Trans. 3 (1972) 627.
[43] B.W. Levinger, Trans. Am. Inst. Min. Met. Eng. 197 (1953) 195.
[44] S.G. Fedotov, N.F. Kvasova, M.I. Ermolova, Dokl. Akad. Nauk SSSR 216 (1974) 363.
[45] L.N. Guseva, L.K. Dolinskaya, Izv. Akad. Nauk SSSR Met. 6 (1974) 195 (In Russian).
[46] B. Straumal, R. Valiev, O. Kogtenkova, et al., Acta Mater. 56 (2008) 6123.
[47] B.B. Straumal, X. Sauvage, B. Baretzky, et al., Scr. Mater. 70 (2014) 59.
[48] B.B. Straumal, A.R. Kilmametov, Yu.O. Kucheev, et al., Mater. Lett. 118 (2014) 111.
[49] B.B. Straumal, V. Pontikis, A.R. Kilmametov, et al., Acta Mater. 122 (2017) 60.
[50] X. Sauvage, F. Wetscher, P. Pareige, Acta Mater. 53 (2005) 2127.
[51] T. Ungar, E. Schafler, P. Hanak, S. Bernstorff, M. Zehetbauer, Mater. Sci. Eng. A 462 (2007) 398.
[52] A.R. Kilmametov, G. Vaughan, A.R. Yavari, et al., Mater. Sci. Eng. A 503 (2009) 10.
[53] T. Ungár, E. Schafler, P. Hanák, et al., Z. Met. 96 (2005) 578.
[54] M. Zehetbauer, E. Schafler, T. Ungár, Z. Met. 96 (2005) 1044.
[55] M.B. Kerber, M. Zehetbauer, E. Schafler, et al., JOM 63 (2011) 61.